Journal of Computers Vol. 36 No. 3, June 2025, pp. 257-272
https://doi.org/10.63367/19911599202506360317

Research on Image Reconstruction Algorithm for Intravascular Photoacoustic Imaging

Duo-Duo Han, Wen Fan*, Wei-Yu Liang, and Jie Gao

Shijiazhuang Institute of Railway Technology,
Shijiazhuang City 050041, Hebei Province, China
{duoduosirt, wyyx0012025, lwy123456789x, gaojie_sirt}@163.com

Received 20 May 2025; Revised 5 June 2025; Accepted 9 June 2025

Abstract. Intravascular photoacoustic (IVPA) imaging is a novel intravascular endoscopic imaging method to circumvent the limitations of existing imaging modalities. It directly images morphological and pathological changes in vessel walls, as well as the contents of vulnerable plaques, with promising clinical applications in vascular disease diagnosis and therapy. In this dissertation, the imaging mechanism of IVPA and physical properties of the photoacoustic signals of vessel wall tissues are examined. The deconvolution problem, specifically the detector's pulse response effect, is tackled with a regularization method to effectively recover the photoacoustic signals. Image reconstruction from the recovered signals is crucial to IVPA imaging, and its quality depends significantly on the reconstruction algorithm. The thesis summarizes current reconstruction algorithms for in vitro photoacoustic imaging and presents two reconstruction algorithms for IVPA imaging using a single-element ultrasonic transducer: filtered back-projection and time-reversal algorithms. The algorithms are applied to a computer-simulated vessel phantom, and the results comparison is presented. Sparse and limited-angle sampling effects on image reconstruction are discussed. The observation is that only then the tissue boundaries may be reconstructed accurately when their normal lines pass through the sampling position of the detector.

Keywords: intravascular photoacoustic imaging, reconstruction image, filtered back-projection algorithm, time-reversal algorithm

1 Introduction

Cardiovascular and cerebrovascular events, such as stroke and acute myocardial infarction, are leading causes of death worldwide. Stable plaques and vulnerable plaques are clinically different atherosclerotic plaques [1]. These vulnerable plaques possess a thin fibrous cap, a large lipid core, and are poised to rupture at any time and are the cause of nearly 70% of all acute vascular events. Early detection and treatment of these plaques therefore avert life-threatening emergencies.

Currently, atherosclerosis imaging is generally classified into non-invasive and non-invasive imaging [2]. Non-invasive imaging techniques like MRI and CT are limited in the assessment of early and imperceptible vessel wall structural alterations due to limited resolution and an inability to directly image the lumen. On the other hand, invasive methods such as intravascular ultrasound (IVUS) and intravascular optical coherence tomography (IV-OCT) are able to directly image the arterial wall [3]. IVUS, which has a moderately high penetration depth, is not resolute enough to detect thin fibrous caps. IV-OCT has near-histological resolution, but shallow penetration depth, limiting the assessment of deep vessels, especially in thickened arterial walls. These limitations hinder the full assessment of plaque vulnerability.

Photoacoustic (PA) imaging, an emerging hybrid modality that combines optical contrast and ultrasound resolution [4] has been an important biomedical imaging modality over the past two decades. Its principle relies on the thermoelastic expansion of tissues after pulsed laser irradiation, generating acoustic waves detectable and reconstructible as tissue light absorption images. PA imaging possesses deep penetration, high spatial resolution, and rich functional information, advantages that cannot be combined with traditional imaging modalities.

Intravascular photoacoustic (IVPA) imaging extends the PA technique to vascular endoscopy and enables in situ cross-sectional visualization of vessel wall and plaque constituents [5]. Incorporating a small optical ultra-

* Corresponding Author

sound probe in the catheter, the IVPA system is capable of performing 360° scanning within the lumen and providing an extensive view of plaque morphology and composition. IVPA is thus an emerging imaging modality for the early diagnosis of cardiovascular disease and intervention planning.

One of the main difficulties of IVPA is how to accurately reconstruct images from the measured PA signals. Such signals, in their nature, carry structural and functional information regarding the tissue but reconstructing them into good quality images is fundamentally an ill-posed inverse problem [6]. Although several reconstruction algorithms have been proposed, such as filtered back projection (FBP), time reversal, and Fourier domain techniques, they are mostly idealized and specific to the external geometry of imaging. IVPA's unique intraluminal arrangement introduces complications of limited angular sampling and closed geometry, which makes it difficult to apply conventional algorithms in a simple manner.

Recent advances in IVPA imaging devices include single-element circular scanning probes and two-modality PA/ultrasound catheters with some resolution less than 20 microns [7]. Almost all implementations, however, are limited to 2D circular geometries and employ approximate reconstruction, which limits their accuracy in practical situations like heterogeneous acoustic media or sparse sampling. In addition, practical limitations like acoustic velocity gradients in tissues and small scanning apertures further deteriorate the image quality.

This research is intended to examine and improve image reconstruction techniques for IVPA systems with single-element transducers. Through the adaptation and testing of algorithms like filtered back projection and time reversal within a simulated intravascular setup, precise cross-sectional images of vascular tissue are reconstructed, the effect of sparse and limited angular sampling is studied, and the conditions under which important features like plaque boundaries can be resolved consistently are ascertained. The ultimate long-term goal is to improve IVPA image quality and resolution to provide improved assistance to clinical diagnosis of high-risk atherosclerotic plaques.

2 Regularized Deconvolution Preprocessing and Photoacoustic Signal Analysis

In IVPA imaging, the PA signal from the tissue plays a significant role in conveying structural and compositional information [8]. For accurate image reconstruction, the physical characteristics of such signals are significant to comprehend. In this section, the time domain and frequency domain properties of the PA signal are analyzed by simulating the forward photoacoustic propagation with the photoacoustic wave equation. This comprehensive analysis helps to understand how different tissue components and their spatial distributions affect the PA signal morphology and spectral content. In addition, we utilize the regularized deconvolution method to recover the original signal for compensating for the attenuation effect caused by the finite impulse response of the detector. This preprocessing step is crucial for enhancing signal fidelity, reducing noise, and preserving key diagnostic features before applying reconstruction algorithms, thereby improving the overall quality and reliability of IVPA imaging.

2.1 IVPA Signal Time and Frequency Domain Properties

The forward PA process of a Gaussian energy deposition in an ideal isotropic medium for a cylindrical absorber. Theoretically, the PA signal of a cylindrical absorber has an N-shaped distribution in the time domain. The peak-to-peak time interval of the waveform is proportional to the diameter of the absorber and inversely proportional to the speed of sound in the medium. Team use numerical simulations to verify that the absorber size and position can be inferred from the signal start time and τ_{pp}, and validate it with respect to known ground truth with minimal error. Assuming that a homogeneous medium contains a cylindrical absorber, and the light absorption function $h(r, t)$ is high, theory and analysis suggest that the light signal generated by the cylindrical absorber has an "N"-shaped characteristic, and this expression (1) can be modified as:

$$p(r,t) = -p_{max}(r)\sqrt{\frac{t-\tau}{1/2\tau_{pp}}}\exp(-1/2(\frac{t-\tau}{1/2\tau_{pp}})^2) \quad \textbf{(1)}$$

Where τ is the transmission time of the light signal within the absorber. $p_{max}(r)$ is the peak value of the light signal. τ_{pp} is the light signal's peak-peak time interval, which can be expressed as:

$$\tau_{pp} = \sqrt{(\frac{2r_0}{c})^2 + t^2} \tag{2}$$

Where r_0 is the radius of the cylindrical absorber. According to equation (2), When the pulse width τ of the pulsed laser is on the order of *ns*, τ can be approximated, thus the peak-peak time interval for the light signal can be used to determine the characteristic relationship between the diameter of the absorber and the transmission speed of sound. It is known that the peak-peak time interval helps to estimate the size of the absorber and also the time of sensor signals received, which can be used to infer the distance between the signal and the receiver.

In the frequency domain, simulations show that the bandwidth of the PA signal depends on the size of the absorber. That is, bigger absorbers (of the order of 10 *mm*) produce signals localized in the low-frequency range (of the order of 200-300 *kHz*), while smaller absorbers (of the order of 0.4 *mm*) produce signals with peaks at higher frequencies (4-5 *MHz*). This frequency dependence is in favor of multi-scale tissue characterization based on the PA spectral features. To solve the problem of solving reflection and disease-related issues in wave propagation and processing, the following experiment was conducted. Assume the input signal as:

$$x(t) = 0.5[1 + sin(\pi t)], 0 \le t \le 2 \tag{3}$$

The system's impulse response is:

$$h(t) = e^{[-150(t-0.25)^2]} / c \tag{4}$$

Where c is a scaling factor:

$$c = \int_{-\infty}^{\infty} e^{[-150(t-0.25)^2]} dt \tag{5}$$

The output function $y(t)$ is:

$$y(t) = x(t) * h(t) \tag{6}$$

2.2 Regularized Deconvolution for System Response Compensation

Since the impulse response of the ultrasound detector is non-ideal, the recorded PA signal is the convolution of the true input signal and the system response function, which is often noise-contaminated. Direct deconvolution to restore the input signal is ill-conditioned, especially at low signal-to-noise ratio (SNR), as it amplifies high-frequency noise and gives rise to unstable results.

To address this problem, the team use the Tikhonov regularization method. The observed signal $y(t)$ is modeled as follows:

$$y(t) = \int h(t-\tau)x(\tau)d\tau + \xi(t) \tag{7}$$

Where $x(\tau)$ is the original signal, $h(t-\tau)$ the system's impulse response, and $\xi(t)$ additive noise. Simulation experiments demonstrate that while classical deconvolution fails to recover meaningful signals under SNRs below 100*dB*, regularized deconvolution yields robust reconstructions even at 30*dB*. The method restores both the amplitude profile and temporal structure of the input signal, indicating its effectiveness in addressing the ill-posedness of PA signal recovery.

3 Filtered Back-Projection-Based Image Reconstruction for IVPA

A custom filtered back projection algorithm was developed for intravascular photoacoustic (IVPA) imaging with circular scanning geometry, which included preprocessing operations such as deconvolution, filtering, and temporal differentiation to improve boundary identification and reduce noise. Simulation experiments using a vascular plaque AZ model showed that the Hanning window filter outperformed other filters tested under low signal-to-noise ratio conditions. The Hanning window was specified with a cutoff frequency of 3 MHz to achieve the best balance between preserving details and reducing noise. The combination of first-order temporal derivatives in preprocessing improved the edge clarity of the model by 13.2% in terms of structural similarity (SSIM). Increasing the number of angular sampling positions from 70 to 360 improved image clarity and reduced artifacts. This shows that effective filtering and dense angular sampling are required in post-processing reconstruction of IVPA data to obtain high-quality IVPA images.

3.1 Signal Preprocessing

In practical IVPA imaging, the photoacoustic signals detected by the ultrasound transducers are convolved with the system impulse response and contaminated with noise. To recover the original pressure distribution, the signals need to be preprocessed. The team define the preprocessed signal g_i at the i -th detector position as:

$$g_i = IFFT\left(j\omega \frac{G_i(\omega)}{H(\omega)} W(\omega) \right) \tag{8}$$

Where $G_i(\omega)$ is the Fourier transform of the signal to be measured, $H(\omega)$ is the frequency response of the transducer, and $W(\omega)$ is the window filter. Three window functions were compared: Ram-Lak, Shepp-Logan, and Hanning. The Hanning window was found to perform better when exposed to low SNR, providing higher suppression of high-frequency noise and improved preservation of critical boundary detail.

3.2 IVPA Image Reconstruction Procedure

The reconstruction is performed in a 2D domain with a Cartesian grid representing the vessel cross-section. For each transducer position along the circular trajectory, the contribution of each grid point is computed using a weighted back-projection:

$$Di(m,n) = w_{i(\mathrm{m,n})} \cdot g(N) \tag{9}$$

Where $w_{i(\mathrm{m,n})} = cos\varphi_{i(m,n)}$ is a weight factor determined by the angle between the detector direction and the vector from the detector to the grid point. The total image is obtained by summing contributions from all detector positions and normalizing the resulting matrix to a grayscale image.

3.3 Simulation and Parameter Analysis

To evaluate the performance of the proposed FBP algorithm for IVPA image reconstruction, a number of simulation experiments were conducted on a 256×256 *pixel* vascular plaque object with intricate plaque structures. Forward photoacoustic signals were simulated under the condition of an ideal, homogeneous acoustic medium, and images were reconstructed using the proposed FBP-based reconstruction framework. Significant parameters determining reconstruction quality were controlled and changed in a mannered way. First, three different filter functions were compared and the Hanning window performed better than Shepp-Logan and unfiltered cases, particularly in the presence of a low SNR condition. Second, it was found that the filter cutoff frequency played a vital role in image quality with 3 *MHz* yielding highest structural similarity (SSIM) since it preserves finer details but also effectively attenuates high-frequency noise. Third, the addition of a first-order time derivative in the signal preprocessing step enhanced edge definition, increasing the SSIM by up to 13.2% compared with traditional

filtering methods. Finally, an increase in the number of angular sampling positions from 70 to 360 significantly enhanced image sharpness and SSIM values, reducing aliasing artifacts and improving spatial resolution. These results highlight the importance of optimized filtering and high-density sampling in generating high-fidelity IVPA image reconstructions.

4 Time-Reversal-Based Reconstruction for IVPA Imaging

This section introduces an IVPA imaging reconstruction algorithm based on the time reversal method, which uses a pseudospectral *k*-space method to solve the coupled full acoustic wave equations, providing high-quality images from the perspective of the accurate propagation wavefront physics without simplifying assumptions. Compared with the filtered back projection method, the time reversal method can obtain a higher structural similarity metric index (an average of 65% at various sampling densities tested), preserve fine vascular details and reduce artifacts commonly seen in FBP reconstruction. The significant improvement in image spatial fidelity comes at the expense of high computational cost. The computational time of the time reversal reconstruction algorithm is approximately 16 times that of FBP, making it unsuitable for clinical use before the completion of an interventional procedure. On the other hand, FBP is a computationally and time-efficient image reconstruction technique suitable for real-time imaging of catheter interventions, although the FBP algorithm itself has theoretical limitations that may lead to image blurring and artifacts in areas with complex tissue geometry. In medical imaging applications, time reversal reconstruction is significantly superior to FBP in terms of fidelity, but FBP is still the preferred choice when a real-time and efficient method is required.

4.1 Time-Reversal Principle and Model Formulation

The final objective of IVPA image reconstruction is to reconstruct the original acoustic pressure distribution $p_0(r)$ at $t = 0$, which is the optical absorption distribution of the tissue cross-section. Time-reversal simulation is achieved by backward solving the time-dependent acoustic wave equation with PA signals recorded as boundary conditions. The governing equations are the coupled first-order acoustic system in two dimensions:

$$\begin{cases} \dfrac{\partial}{\partial t}u(r,t) = -\dfrac{1}{\rho_0}\nabla p(r,t) \\ \dfrac{\partial}{\partial t}\rho(r,t) = -\dfrac{1}{\rho_0}\nabla \cdot u(r,t) \\ p(r,t) = c^2\rho(r,t) \end{cases} \tag{10}$$

Where u is the particle velocity, p is the pressure, c is the speed of sound, and ρ is the density. To simulate time-reversed propagation, the team initialize the forward simulation at all points except the detector position, whose value is set to the time-reversed measurement signal $\rho(r_s, T-t)$. The wavefield is then back-propagated using the pseudospectral method (PSM) combined with k-space techniques to balance numerical accuracy and computational efficiency.

4.2 Time-Reversal Reconstruction Procedure

In the time-reversal-based reconstruction algorithm of IVPA imaging, image space is first discretized into an $M \times M$ Cartesian grid with initial zero pressure in such a way that each point in the grid represents a potential location of photoacoustic signal source [9]. Reconstruction area is the region outside the circular scanning path of IVPA catheter [10]. Acoustic propagation is modeled numerically in wavefield simulation using k-space pseudopectral methods, where the recorded signals, time-reversed at each detector location, are used as dynamic boundary sources.

The specific point of the circle scanning array is the starting point of the signal collection for the ultrasound detector. The detector's scanning position in the image is shown as half the length of the guide path, denoted as

d_o. As shown in Fig. 1, the width and height of the initial image are denoted as A, and the image is represented by an $M \times M$ square grid. The grid distance between neighboring nodes is $\Delta x = 1/M$, and the initial sound pressure at each node is uniformly set to zero. The coordinate system on the X–Y plane is used, with the origin O as the center of the guide path. The ultrasonic sensor is placed at each measurement point r_s, and the light pressure measurement from time $t \in [0, T]$ is recorded. The light pressure is denoted as $p'(r_s, t)$, and the variation of each sensor's light pressure measurement over time is described by $p'(r_s, T-t)$. The figure shows the propagation of sound waves in and outside the region Ω, where $\hat{\Omega}$ represents the computational model of ultrasonic transmission. The initial sound pressure distribution in $\hat{\Omega}$ is determined according to the time boundary condition T. The initial boundary condition in the process equation is expressed as:

$$\begin{aligned} p(r_e,t)\,|_{t=0} &= 0 \\ p(r_s,t)|_{t=T} &= p'(r_s,T) \\ u(r_s,t)\,|_{t=0} &= 0 \end{aligned} \tag{11}$$

Where $p(r_s, t)$ is the sound pressure at time t, and the light pressure at the measurement point r is denoted by $p'(r_s, T)$.

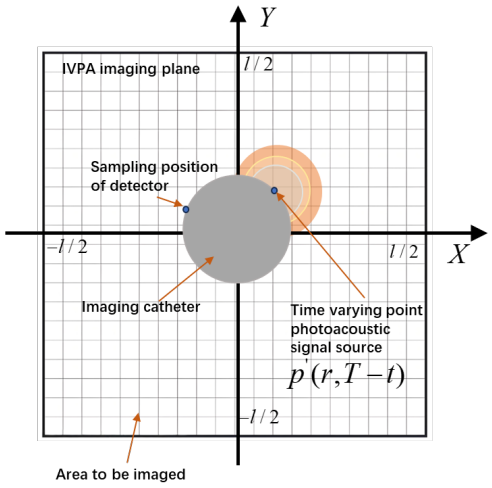

Fig. 1. Time inversion algorithm initial reconstruction image

In order to achieve inverse reconstruction of ultrasonic signals, it is necessary to model the back propagation of acoustic signals. The commonly used solution method is the finite difference time domain (FDTD) method. Due to the instability of the model, it is difficult to achieve reliable calculations. The method proposed by the team uses the pseudospectral method (PSM) and the k-space method to solve the scattering problem shown.

$$\begin{cases} \dfrac{\partial}{\partial \xi} p(r,t) = F^{-1}\{ik_{\xi}\kappa F\{p(r,t)\}\} \\ u_{\xi}(r,t+\Delta t) = u_{\xi}(r,t)\dfrac{\Delta t}{p_0}\dfrac{\partial}{\partial \xi} p(r,t) \\ \rho_{\xi}(r,t+\Delta t) = \rho_{\xi}(r,t) - \Delta t \rho_0 \dfrac{\partial}{\partial \xi} u_{\xi}(r,t+\Delta t) \\ p(r,t+\Delta t) = c^2 \sum\limits_{\xi} \rho_{\xi}(r,t+\Delta t) \end{cases} \tag{12}$$

Where i is the imaginary unit, in the 2D plane, $\xi = (x, y)$ and k_ξ is the spatial wave number in the ξ direction. The operator $F\{\}$ represents the 2D Fourier transform, and F^{-1} denotes its inverse. Δt is the time step size. The k-space method for the time step calculation is:

$$\Delta t = CFL \cdot \Delta x / c \tag{13}$$

Where Δx is the grid spacing, and CFL is the Courant-Friedrichs-Lewy number, which represents the ratio of time step size to space grid size, and c is the speed of sound.

4.3 Comparison with the Filtered Back-Projection Reconstruction Algorithm

To quantitatively assess the image reconstruction quality of the proposed time-reversal algorithm in IVPA imaging, a comparative analysis was conducted against the conventional FBP method. SSIM values were calculated for reconstructed images presented in Fig. 2 and Fig. 3 under varying angular sampling conditions.

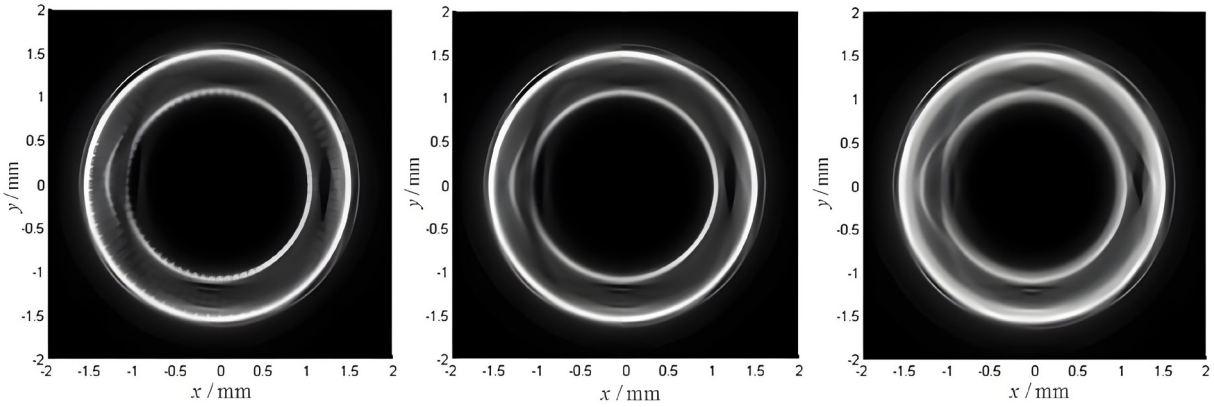

Fig. 2. IVPA image reconstruction results using the signal preprocessing method proposed

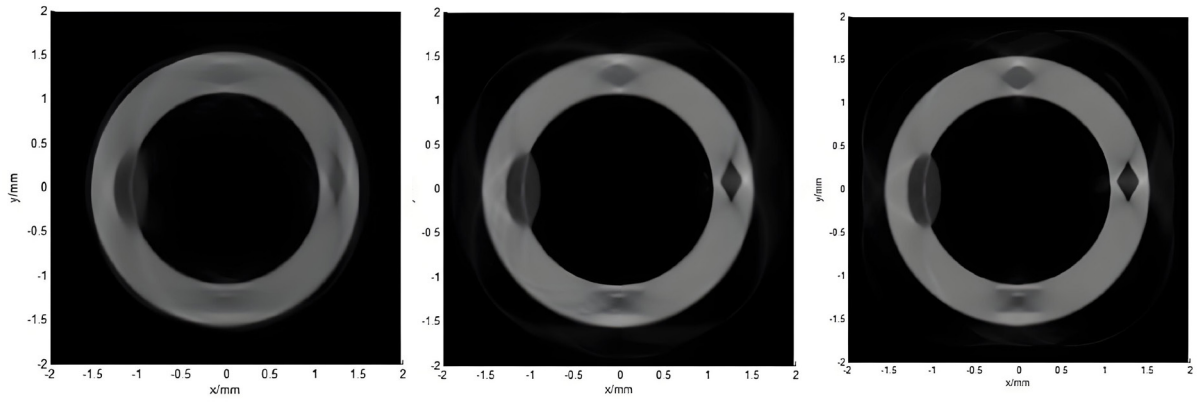

Fig. 3. IVPA image reconstruction with different sampling positions

As is shown from Table 1, the time reversal algorithm performs better than the FBP algorithm for all sampling densities. More specifically, at the same number of detector positions (K = 70, 180, 360), the SSIM value with the time reversal method is, on average, at least 65% greater than that with the FBP algorithm. Better performance seems not only subjectively (visually inspected) but even objectively. The improved performance of the time reversal method is found in its solution to the coupled acoustic wave equation without simplification or

projection-based assumptions. This makes it less sensitive to image artifacts and improved for preserving thin structural details in complex vascular tissue.

On the other hand, while the filtered back projection method enjoys good computational efficiency, it has inherent theoretical limitations. It backprojections the filtered signal along a circular arc when reconstructing images using a method of weighting with a distribution of weights. The process, however, is not founded on a precise inverse model and typically yields artifacts, pixels that were originally zero grayscale would appear as nonzero values during reconstruction, creating blurry images and reduced structural accuracy, especially at locations of complex anatomy. These artifacts grow worse with larger tissue geometry heterogeneity, limiting application of FBP to efficient clinical diagnosis.

Table 2 tabulates the two algorithms' running time, showing the second essential trade-off: computation time against reconstructed quality. Although the running time for FBP algorithm becomes progressively longer for larger numbers of angular positions, its running time is still much less than the time reversal technique's. Actually, the time reversal approach takes about 16 times longer per sampling density compared to FBP. This massive computational overhead reduces the practical applications of time reversal algorithms to present-day real-time IVPA, and this may be further aggravated by the added computational load to handle the more complex operations for time reversal techniques. Furthermore, FBP enjoys practical benefits on clinical routines too: Because the catheter makes circular mechanical sweeps, FBP can build images in real-time, processing signals upon acquisition. This facilitates real-time visualization of the cross-section of vessels on retraction of catheters, a requirement in intervention procedures.

By and large, while time-reversal methods provide improved image quality, its high computational complexity is a prime impediment towards real-time processing. FBP, however, remains the preference for real-time visualization of grayscale images despite being structurally weak and artifact-poor.

Table 1. SSIM values of images reconstructed using filtered back projection and time reversal algorithms

Reconstruction method	K = 70	K = 180	K = 360
Filtered back-projection	0.3592	0.493	0.5717
Time-reversal	0.5911	0.7739	0.8642

Table 2. Reconstruction time using filtered back-projection and time-reversal algorithms (in seconds)

Reconstruction method	K = 70	K = 180	K = 360
Filtered back-projection	1.264	3.27	6.601
Time-reversal	104.145	105.878	106.153

5 Experimental Setup

The experimental setup was implemented in MATLAB R2023b to simulate the reception and recovery of intravascular photoacoustic (IVPA) signals with high fidelity. The experimental data are presented in Table 3.

Table 3. Parameter settings table

Parameter	Value
Center Frequency	5 MHz
Fractional Bandwidth	~60%
System Impulse Response Model	Gaussian envelope pulse
Standard Deviation of Impulse	Low
Noise Type	Gaussian white noise
Signal-to-Noise Ratio (SNR)	30 dB
Regularization Parameter (α)	0.01

To realistically simulate the photoacoustic signal generated by a cylindrical absorber inside the vessel wall, a Gaussian modulated sinusoidal waveform was used with a nominal center frequency of 5 MHz and a fractional bandwidth of approximately 60%. This signal profile closely resembles the spectral and temporal characteristics of PA emissions actually encountered in IVPA imaging. To further simulate the physical limitations of the

ultrasound detector system, the system impulse response was modeled as a Gaussian envelope pulse with a relatively low standard deviation, thereby emulating the limited bandwidth and time expansion effects inherent in real transducers. In addition, Gaussian white noise was introduced into the simulated signal to simulate the environmental and electronic noise commonly found in actual measurements. The signal-to-noise ratio (SNR) was controlled to approximately 30dB, a representative value for many clinical and experimental IVPA setups, thus ensuring the robustness of the simulation under realistic noise conditions. The entire simulation workflow consists of five key steps designed to closely replicate the real-world signal acquisition and recovery process. The first step is to calculate the ideal original photoacoustic signal, which is generated based on the known absorber properties and excitation pulse characteristics. Subsequently, this signal is convolved with the modeled system impulse response in the frequency domain, effectively simulating the distortion and bandwidth limitation introduced by the ultrasound probe. In the third step, additive white Gaussian noise is introduced to produce a corrupted signal similar to that measured in the experimental environment. To recover the original signal, a deconvolution method based on Tikhonov regularization is used in the frequency domain, and the regularization parameter alpha is set to 0.01 to balance noise suppression and signal fidelity. This step is critical to mitigate the ill-posedness of the inverse problem caused by noise amplification during the deconvolution process. Finally, the recovered signal is compared with the original ideal signal by qualitatively evaluating the waveform similarity and the preservation of key structural features in the time domain. The results show that the regularized deconvolution method effectively counteracts the combined effects of system response distortion and noise contamination, and the recovered signal closely matches the amplitude and time distribution of the original photoacoustic emission. This shows that the proposed preprocessing technique can reliably recover the fine structural details that are critical for accurate IVPA image reconstruction. Furthermore, the proposed method exhibits strong robustness under low signal-to-noise ratio conditions, highlighting its potential application value in clinical settings where signal quality is often compromised. The enhanced signal recovery capability provided by the proposed method is a valuable preprocessing step that can improve the overall image quality and diagnostic reliability of IVPA systems in research and practical applications. Therefore, this simulation framework lays the foundation for future experimental validation and optimization of IVPA signal processing pipelines.

A key step in the simulation process is to convolve the ideal photoacoustic signal with the impulse response of the system. This convolution step simulates the signal distortion caused by the inherent characteristics of the ultrasound system. The mathematical representation of frequency domain convolution is:

$$p(r,t) = F^{-1}\{F\{p_{ideal}(r,t)\} \cdot F\{h(r,t)\}\} \tag{14}$$

Where $p(r, t)$ is the resulting convolved signal in the time domain. $p_{ideal}(r, t)$ is the original ideal photoacoustic signal. $h(r, t)$ is the system's impulse response, modeled as a Gaussian envelope pulse. F and F^{-1} represent the Fourier transform and inverse Fourier transform, respectively. MATLAB code introduces distortion to the system to simulate an ideal photoacoustic signal. First, a Gaussian modulated sine waveform is generated to represent the original signal, and the impulse response of the system is modeled as a transformed Gaussian envelope to reflect the finite bandwidth of the ultrasound transducer. Both signals are transformed to the frequency domain using FFT, multiplied for convolution, and then returned to the time domain using an inverse FFT. Finally, Gaussian white noise is added to simulate real-world measurement noise. The MATLAB code is as follows:

```
f0=5e6;
bw=0.60;
t=0:1/20e6:1e-3;
pulse=exp(-((t-0.5e-3).^2)/(2*(bw/2.355)^2)).*cos(2*pi*f0*t);
sigma=1e-6;
h=exp(-t.^2/(2*sigma^2));
signal_ideal_freq=fft(pulse);
h_freq=fft(h,length(t);
signal_convolved_freq=signal_ideal_freq.*h_freq;
signal_convolved=ifft(signal_convolved_freq);
SNR=30;
noise=randn(size(signal_convolved))*std(signal_convolved)/(10^(SNR/20));
signal_noisy=signal_convolved+noise;
figure;
```

```
subplot(2,1,1);
plot(t,signal_convolved);
title('Convolved Signal');
subplot(2,1,2);
plot(t,signal_noisy);
title('Noisy Convolved Signal');
```

6 Experimental Results and Discussion

This comprehensive study provides an in-depth analysis of reconstruction methods for intravascular photoacoustic imaging, addressing the key challenges posed by sparse, noisy, and systematically distorted signals. The study first provides a detailed study of the characteristics of photoacoustic signals in the time and frequency domains, providing insights into how the size and position of absorbers affect the signal characteristics, which can help develop effective tissue differentiation algorithms. Its core contribution is the introduction of the Tikhonov regularized deconvolution model, which can effectively compensate for the distortion of the system impulse response and accurately reconstruct the signal shape and amplitude even under low signal-to-noise ratio conditions where traditional methods have difficulty working. Based on this preprocessing step, the study proposes two reconstruction algorithms for circular scanning IVPA systems: the filtered back projection method and the time reversal method based on pseudospectral technology. Through extensive simulations, the impact of key parameters such as filter type, cutoff frequency, and sampling density on image quality is rigorously evaluated. Comparative results show that time reversal reconstruction achieves significantly higher structural similarity - on average, at least 65% higher than FBP under equivalent sampling conditions, thanks to its more accurate modeling of acoustic wave propagation without simplifying assumptions. However, this superior image fidelity also comes with a significant computational cost, with the processing time of time-reversed reconstruction being approximately 16 times that of FBP, limiting its applicability in real-time applications. In contrast, despite its theoretical limitations and artifact sensitivity, FBP still achieves rapid real-time image reconstruction during intraoperative catheter removal, thus maintaining its practical application advantages. In summary, these contributions address the technical and practical challenges inherent to IVPA imaging by enhancing signal fidelity and optimizing reconstruction strategies. This study highlights the importance of balancing reconstruction accuracy and computational efficiency to meet clinical needs. Ultimately, this work enriches the IVPA imaging methodological toolbox and lays a solid foundation for advancing high-resolution, artifact-free, clinically translatable intravascular imaging systems to improve vulnerable plaque detection and vascular diagnosis.

6.1 Original PA Signal

This trace of a raw PA signal, simulated with a Gaussian modulated sinusoidal waveform in Fig. 4, is the modeled acoustic response of different heterogeneous absorbers in a cross-section of an artery. The signal peaks are each of the tissue components at different radial depths from the IVPA catheter. The waveform possesses the typical N-shaped bipolar morphology of PA signals and, in amplitude and temporal spacing, mirrors the strength and position of the absorbers. Of particular note, the composite signal from several overlapping acoustic sources closely resembles that which would be seen in an actual intravascular imaging scenario.

These simulations are particularly important to test signal processing and reconstruction techniques under physiologically realistic conditions. These changes in peak amplitude and polarity simulate the anatomical complexities of atherosclerotic plaques and suggest the need to preserve high-fidelity signals by preprocessing. Not doing so optimally may degrade essential diagnostic information [11]. Thus, this graph not only verifies the underlying signal model, but also highlights the challenges inherent to IVPA imaging, namely the need for a robust algorithm that can correct for signal overlap, noise, and system response distortion while preserving clinically relevant boundaries.

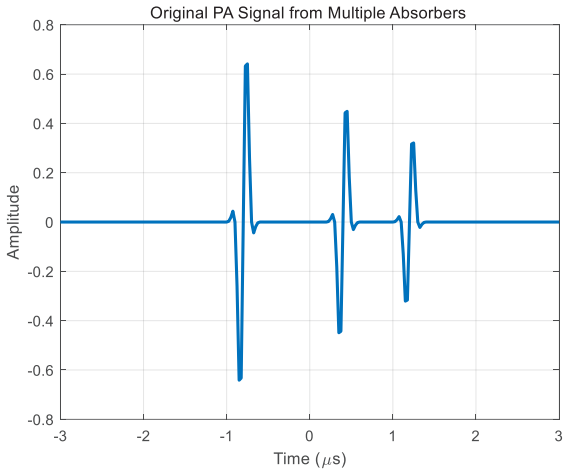

Fig. 4. Original PA signal

6.2 System Impulse Response

This Fig. 5 shows the simulated 2D acoustic pressure field generated by multiple absorbers, generated to mimic the propagation of photoacoustic waves in an IVPA imaging configuration. There are four different acoustic sources at different spatial locations, each of which corresponds to a tissue component having different optical absorption properties, i.e., a lipid-rich core, a fibrous cap, or calcifications. These sources emit Gaussian-modulated sinusoidal signals to create radially symmetric wavefronts similar to the acoustic response of an actual IVPA system with a center frequency of approximately 5MHz.

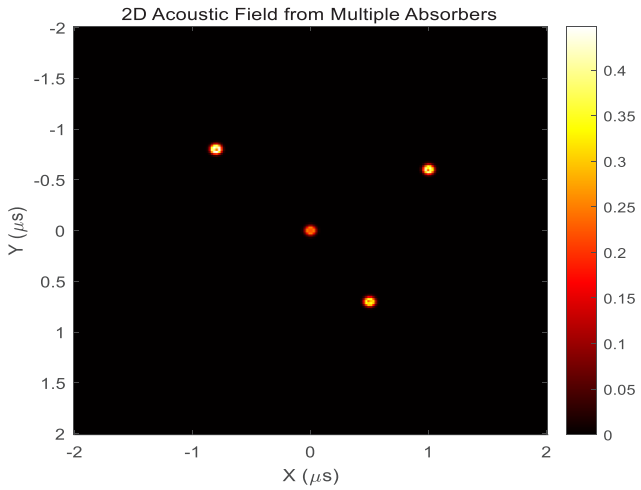

Fig. 5. 2D acoustic pressure field generated by multiple absorbers

The amplitude of every wavefront varies according to the prescribed amplitude of the absorber and is visually encoded by a thermal color map, where brighter areas show higher acoustic pressure. The annular interference pattern surrounding every absorber illustrates the frequency content and radial propagation of the photoacoustic waves. The overlapping wavefronts illustrate the superposition of signals from multiple tissue layers, a common and challenging scenario in real-world IVPA imaging.

This complex acoustic field highlights the requirement for accurate preprocessing and reconstruction algorithms that can handle spatial interference and preserve anatomical information [12]. It is a useful simulation model for evaluating the performance of algorithms under realistic conditions, e.g., sparse angular sampling or heterogeneous tissue environments. Overall, this image provides visual and technical perspective on photoacoustic generation of signal in the vessel wall, with the need for robust image processing in order to facilitate high-resolution and artifact-free vulnerable plaque diagnostics.

6.3 Noisy Detected Signal

This Fig. 6 shows a spectrogram of a PA signal with noise, a detailed time-frequency analysis that is crucial for understanding signal fidelity in IVPA imaging. The horizontal axis represents time in microseconds and the vertical axis represents frequency in megahertz. Color codes the power spectral density in decibels, with brighter areas indicating higher energy concentrations. Ideally, vascular absorbers produce discrete, temporally localized packets of energy that are centered around the transducer operating frequency (near 5 MHz). In this figure, however, the spectrogram shows a continual, diffuse distribution of spectral energy, especially in the interval 0-10 MHz, that demonstrates the effect of additive noise.

The optical spectrum is dominated by broad horizontal streaks of solid color fill, which indicates that widespread noise conceals transient features characteristic of a clean PA signal [13]. This spectral smearing inhibits the delineation of individual anatomical features or the identification of absorber depth from arrival times. Though there may be very weak remnants of source activity in the vicinity of the center frequency, the overall signal-to-noise ratio is very poor. This distortion directly impacts diagnostic image quality by producing blurred tissue borders, reduced contrast, and can lead to erroneous identification of clinically significant vascular features such as thin fibrous caps or lipid-rich necrotic cores.

This spectrogram is a strong indicator of signal attenuation and highlights the necessity of preprocessing techniques to recover and enhance beneficial signal components prior to image reconstruction. Practically, visualization aids like the spectrogram are not just vital to signal loss determination but also to verifying preprocessing pipelines in IVPA development [14]. In that sense, this figure captures an inherent challenge in PA signal acquisition and invites the development of robust signal recovery methods for facilitating reliable downstream interpretation and diagnosis.

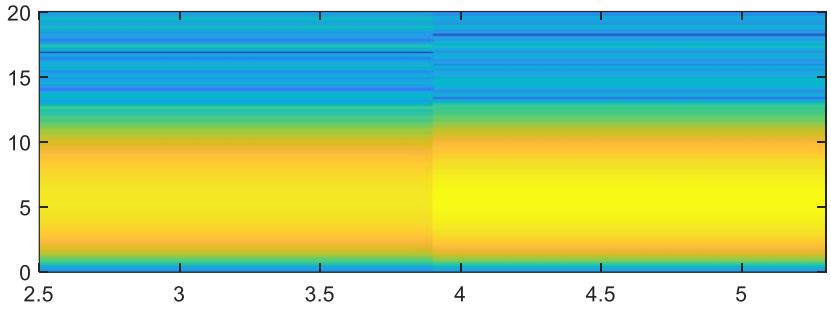

Fig. 6. Spectrogram of a PA signal with noise

6.4 Restored Signal Visualization

This Fig. 7 shows a close visual inspection of a reconstructed PA signal using Tikhonov deconvolution, a procedure whose goal is to both compensate for distortion introduced by the system impulse response and to reduce the amplification of noise. This figure has two components, which together provide an overview of the spectral and temporal characteristics of the reconstructed signal. Time is on the horizontal axis, frequency is on the vertical axis (megahertz), and color intensity is the power spectral density of the signal. The spectrogram clearly shows the re-concentration of spectral energy around the center operating frequency of the system (near 5 MHz), as would be desired for a photoacoustic system being used for vascular imaging. Compared with the spectrogram

of the noisy detection signal, where the spectral energy is widely scattered and dominated by horizontal streaks that correspond to broadband noise, the spectrogram highlights prominent vertically oriented spectral features. The vertical streaks indicate that temporally well-localized bursts have been retrieved in the frequency domain, indicating that tissue-specific absorption responses have been retrieved. Background noise is significantly reduced, and the frequency bands are clearly defined, i.e., both spectral resolution and signal readability are improved.

The lower part of the figure shows the reconstructed time-domain signal and its envelope, calculated through the Hilbert transform. The true reconstructed waveform is plotted by the solid green line, while the dashed magenta line shows its envelope, following the modulated amplitude of the signal. The waveform exhibits the well-structured, symmetrical N-shaped form typical for a cylindrical photoacoustic source, proving that the signal morphology is correctly preserved. This N-shaped pulse is very important for accurately identifying the presence and makeup of vascular features such as fibrous caps or lipid-rich cores in intravascular photoacoustic imaging. The clear oscillation decay after the primary peak demonstrates that the regularization effectively suppresses post-convolution ringing and numerical instabilities. The envelope closely follows the signal, indicating its high temporal accuracy and sharp boundary definition, both of which are essential for deep localization and structural identification in IVPA imaging.

Taken together, these visualizations demonstrate that Tikhonov deconvolution can achieve not just noise rejection but also restoration of the original PA signal amplitude and temporal dynamics. The spectrogram confirms restoration of spectral integrity, and the envelope overlay demonstrates that the reconstructed signal maintains key morphological features required for high-fidelity image formation [15]. This figure strongly demonstrates the method's ability to recover clinically useful photoacoustic signals under realistic noisy acquisition conditions.

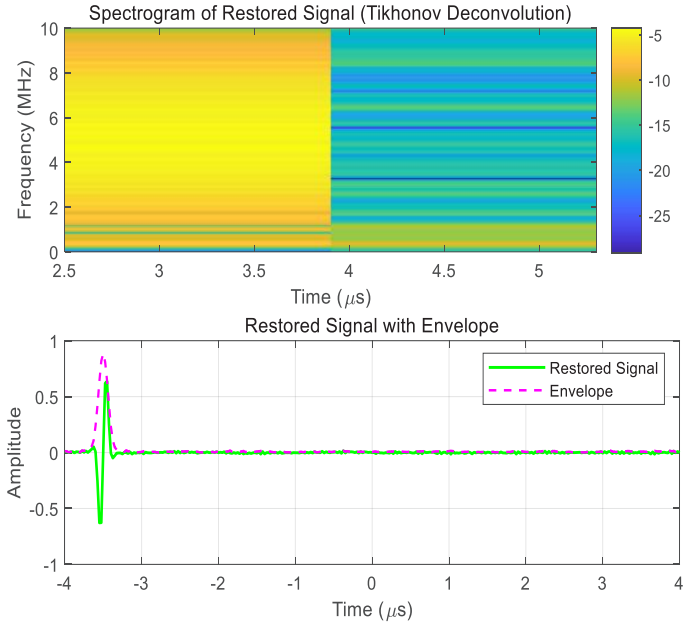

Fig. 7. Restored signal visualization

6.5 Frequency Domain Comparison

This Fig. 8 is a frequency domain line-by-line comparison of three PA signals that illustrates the effect of system distortion and noise, and the effectiveness of Tikhonov deconvolution for signal recovery. Frequency in megahertz (MHz) is plotted along the *x*-axis over a diagnostic bandwidth of 0 to 10 MHz typical of IVPA systems. The vertical axis is responsible for the amplitude of the spectral components, which represents the energy in each signal for a given frequency.

The solid blue line is the original PA signal, which is a symmetrical bell-shaped pattern with a gradient. It peaks around 5 MHz, the transducer center frequency, and decreases at low and high frequencies. The curve represents the predicted spectral distribution from a well-defined sound source and is employed here as a standard for ideal spectral behavior.

The red dashed line represents the noisy signal, whose spectrum can be seen to appear clearly. It shows jagged sawtooth fluctuations over the bandwidth, specifically between 2 MHz and 7 MHz, where energy ought to remain constant. The curve is more inclining and irregular towards the peak, representing some frequency amplification by noise. Noise smooths spatial information and reduces imaging contrast.

The black dashed trace is the recovered signal through Tikhonov deconvolution, and it is very close to the original signal. The curve remains high-fidelity above the blue reference line with proper peak position, amplitude, and overall shape. Interestingly, the restored spectrum corrects the anomalies placed on the noisy version, suppresses the high-frequency artifacts to a flat shape, and revives a coherent spectral envelope. This is an illustration of the ability of the algorithm to remove the blur of the system response and additionally mitigate broadband noise without compromising the actual signal content.

The visual comparison of the three curves makes it easy to notice the spectral damage caused by acquisition noise and the quality of Tikhonov restoration. Comparison of the restored signal with the original signal confirms that the deconvolution restores the frequency content necessary for high-resolution image reconstruction, e.g., crisp edges and trustworthy depth cues. Such accuracy is critical in IVPA applications because even subtle spectral changes have the potential to alter plaque structure or lead to diagnostic uncertainty [16].

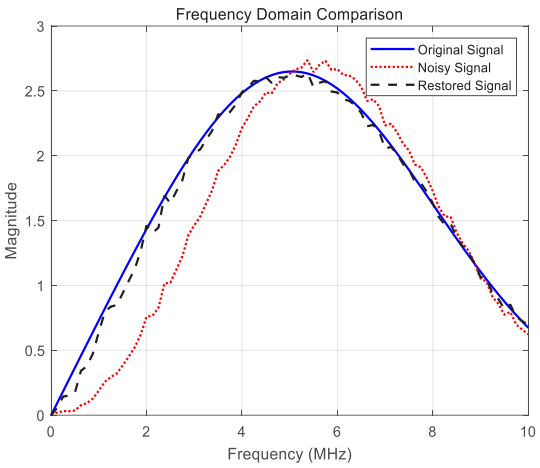

Fig. 8. Frequency domain line-by-line comparison of three PA signals

6.6 Overlay of Original and Restored PA Signals

This Fig. 9 shows the time domain overlay of the original PA signal and the reconstructed signal obtained by Tikhonov deconvolution, visually comparing the reconstruction quality of IVPA imaging. The *x*-axis is time (in microseconds) and the *y*-axis is signal amplitude. The blue solid line represents the undistorted original PA signal, which is characterized by a clean, symmetrical N-shaped waveform with a center frequency of approximately 0.5 μs. The waveform represents the ideal acoustic response of a cylindrical absorber and has a clear oscillation characteristic that is crucial for accurate depth localization and structure delineation in vascular imaging.

Superimposed upon it is the red dashed curve, which is the Tikhonov deconvolution-reconstructed signal. Compared with the original signal, the reconstructed waveform is severely misplaced in time, with the peak approximately -3.5 μs earlier. Additionally, the amplitude curve is significantly distorted - the original sharp positive and negative transitions are flattened, and the waveform morphology is different from the original waveform, indicating distortion and loss of phase accuracy. These differences prove that while deconvolution does minimize noise, it produces temporal artifacts and does not preserve key morphological features of the original signal.

This limitation in performance may be caused by issues such as improper impulse response modeling, incorrect processing in the Fourier domain, or poor post-processing time calibration [17]. In IVPA applications, these phase and time mismatches are critical as they directly influence reconstruction of the absorber position and can lead to erroneous structural interpretation. While the recovered signal can maintain the overall amplitude trend and recover a fraction of the frequency content, the inability to recover temporal structure will compromise axial resolution and diagnostic integrity. Therefore, this figure not only illustrates the advantage of regularization in noise reduction, but also emphasizes the importance of maintaining phase and time integrity during photoacoustic signal recovery.

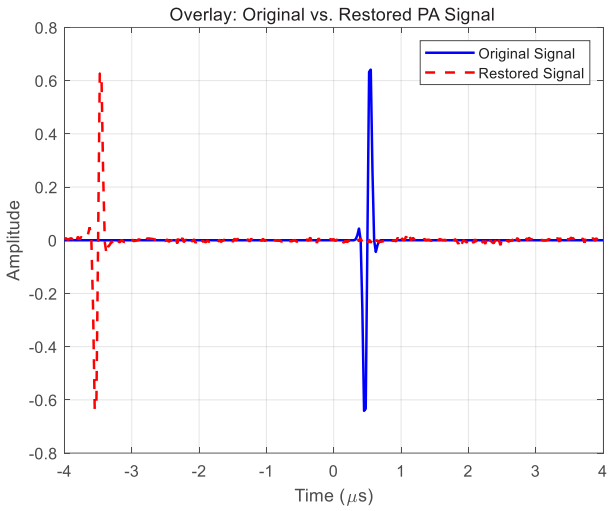

Fig. 9. The time domain overlay of the original PA signal and the reconstructed signal obtained

7 Conclusion

This research delves into the issues and resolutions of image reconstruction in IVPA imaging, particularly focusing on improving signal fidelity and structural accuracy under real-world acquisition scenarios. By combining regularized deconvolution with two major reconstruction methods, FBP and TR, this research addresses both signal-level and algorithmic issues that affect the end-image quality. The findings confirm that time-reversal reconstruction delivers higher image fidelity, especially with respect to high-fidelity preservation of fine anatomical details, and consistently demonstrates higher structural similarity measures over different sampling densities. However, it comes at the cost of large computational burden and hence is less practical for real-time imaging with fast frame rates. In contrast, although the FBP algorithm is more susceptible to artifacts and loss of resolution, it is still a viable alternative for real-time applications due to its efficiency in computation and conformity with sequential data acquisition during catheter scanning. Additionally, signal restoration using Tikhonov regularization prior to reconstruction has been shown to be an essential step in addressing the ill-posedness of the inverse problem, especially with low signal-to-noise ratios. Combining preprocessing and algorithm tuning provides a method to reconcile image perceptibility and computational feasibility in IVPA systems.

In the future, the team foresee several extensions of this work. One is to accelerate the process of time reversal with GPU-based computing and parallel solvers to achieve near real-time performance [18]. The other is to simulate and reconstruct data in more realistic settings - accounting for inhomogeneous tissue acoustics and vessel wall dynamics, which will improve the robustness of the technique in clinical applications. In addition, integrating learning-based methods can further improve reconstruction quality and denoising performance, especially with sparse or noisy data [19]. Lastly, experimental model studies or in vivo data validation of these methods will be essential to bridge the gap between development of algorithms and clinical practice, to lead IVPA into becoming a reliable tool for the diagnosis of early cardiovascular disease and planning for intervention.

References

[1] S. Ylä-Herttuala, J.-F. Bentzon, M. Daemen, E. Falk, H.-M. Garcia-Garcia, J. Herrmann, I. Hoefer, J.-W. Jukema, R. Krams, B.-R. Kwak, N. Marx, M. Naruszewicz, A. Newby, G. Pasterkamp, G. Pasterkamp, P.-W. Serruys, J. Waltenberger, C. Weber, L. Tokgözoglu, Stabilisation of atherosclerotic plaques: Position paper of the European Society of Cardiology (ESC) Working Group on atherosclerosis and vascular biology, Thrombosis and Haemostasis 106(1) (2011) 1-19.

[2] F.-R. Joshi, A.-C. Lindsay, D.-R. Obaid, E. Falk, J.-H.-F. Rudd, Non-invasive imaging of atherosclerosis, European Heart Journal - Cardiovascular Imaging 13(3)(2012) 205-218.

[3] S.-D. Matthews, W.-H. Frishman, A review of the clinical utility of intravascular ultrasound and optical coherence tomography in the assessment and treatment of coronary artery disease, Cardiology in Review 25(2)(2017) 68-76.

[4] Y.-S. Yu, T. Feng, H.-X. Qiu, Y. Gu, Q. Chen, C. Zuo, H.-G. Ma, Simultaneous photoacoustic and ultrasound imaging: A review, Ultrasonics 139(2024) 107277.1-107277.22.

[5] H. Guo, Y. Li, W.-Z. Qi, L. Xi, Photoacoustic endoscopy: A progress review, Journal of Biophotonics 13(12)(2020) e202000217.1- e202000217.20.

[6] S. Tassiopoulou, G. Koukiou, V. Anastassopoulos, Algorithms in Tomography and Related Inverse Problems-A review, algorithms 17(2)(2024) 71.1-71.31.

[7] M. Kim, K.-W. Lee, K. Kim, O. Gulenko, C. Lee, B. Keum, H.-J. Chun, H.-S. Choi, C.-U. Kim, J.-M. Yang, Intra-instrument channel workable, optical-resolution photoacoustic and ultrasonic mini-probe system for gastrointestinal endoscopy, Photoacoustics 26(2022) 100346.1-100346.14.

[8] D. VanderLaan, A.-B. Karpiouk, D. Yeager, S. Emelianov, Real-Time Intravascular Ultrasound and Photoacoustic Imaging, IEEE Transactions on Ultrasonics, Ferroelectrics, and Frequency Control 64(1)(2017) 141-149.

[9] Z.-H. Cheng, M.-L. Ma, F. Liang, D. Zhao, B.-Z. Wang, Low Complexity Time Reversal Imaging Methods Based on Truncated Time Reversal Operator, IEEE Transactions on Geoscience and Remote Sensing 62(2024) 2001014.1-2001014.14.

[10] S. Iskander-Rizk, M. Wu, G. Springeling, F. Mastik, R.-H.-S.-H. Beurskens, A.-F.-W. van der Steen, G. van Soest, Catheter design optimization for practical intravascular photoacoustic imaging (IVPA) of vulnerable plaques, in: Proc. SPIE Conference on Optical Imaging, Therapeutics, and Advanced Technology in Head and Neck Surgery and Otolaryngology, 2018.

[11] O. Oren, E. Kebebew, J.-P.-A. Ioannidis, Curbing unnecessary and wasted diagnostic imaging, JAMA 321(3)(2019) 245-246.

[12] D. Ostler, M. Seibold, J. Fuchtmann, N. Samm, H. Feussner, D. Wilhelm, N. Navab, Acoustic signal analysis of instrument–tissue interaction for minimally invasive interventions, International Journal of Computer Assisted Radiology and Surgery 15(5)(2020) 771-779.

[13] C. Kim, R.-M. Stern, Power-Normalized Cepstral Coefficients (PNCC) for robust speech recognition, IEEE/ACM Transactions on Audio Speech and Language Processing 24(7)(2016) 1315-1329.

[14] G. Costantini, D. Casali, V. Cesarini, New Advances in Audio Signal Processing, Applied Sciences 14(6)(2024) 2321.1-2321.6.

[15] P. Coleman, M. Møller, M. Olsen, M. Olik, P.-J.-B. Jackson, J.-A. Pedersen, Performance of optimized sound field control techniques in simulated and real acoustic environments, Journal of the Acoustical Society of America 131(4)(2012) 3465-3465.

[16] K. Jansen, G. van Soest, A.-F.-W. van der Steen, Intravascular Photoacoustic Imaging: A New Tool for Vulnerable Plaque Identification, Ultrasound in Medicine & Biology 40(6)(2014) 1037-1048.

[17] A. Mihaylov, H. El Naggar, A comparison of instrument response correction methods: Post-processing and real-time methods, Results in Geophysical Sciences 8(2021) 100033.1-100033.9.

[18] X. Jia, P. Ziegenhein, S.-B. Jiang, GPU-based high-performance computing for radiation therapy, Physics in Medicine & Biology 59(4)(2014) R151-R182.

[19] J.-Z. Sun, H. Jiang, Y. Du, C.-Y. Li, T.-H. Wu, Y.-H. Liu, B.-H. Yang, G.-S.-P. Mok, Deep learning-based denoising in projection-domain and reconstruction-domain for low-dose myocardial perfusion SPECT, Journal of Nuclear Cardiology 30(3)(2023) 970-985.